

# Adjusting Logit in Gaussian Form for Long-Tailed Visual Recognition

Mengke Li · Yiu-ming Cheung\* · Yang Lu · Zhikai Hu · Weichao Lan · Hui Huang

Received: date / Accepted: date

**Abstract** It is not uncommon that real-world data are distributed with a long tail. For such data, the learning of deep neural networks becomes challenging because it is hard to classify tail classes correctly. In the literature, several existing methods have addressed this problem by reducing classifier bias provided that the features obtained with long-tailed data are representative enough. However, we find that training directly on long-tailed data leads to uneven embedding space. That is, the embedding space of head classes severely compresses that of tail classes, which is not conducive to subsequent classifier learning. This paper therefore studies the problem of long-tailed visual recognition from the perspective of feature level. We introduce feature augmentation to balance the embedding distribution. The features of different classes are perturbed with varying amplitudes in Gaussian form. Based on these perturbed features, two novel logit adjustment methods are proposed to improve model performance at a modest computational overhead. Subsequently, the distorted embedding

Mengke Li  
Guangdong Laboratory of Artificial Intelligence and Digital Economy (SZ), Shenzhen, China  
E-mail: limengke@gmail.ac.cn

Yang Lu  
Department of Computer Science and Technology, School of Informatics, Xiamen University, China  
E-mail: luyang@xmu.edu.cn

Yiu-ming Cheung · Zhikai Hu · Weichao Lan  
Department of Computer Science, Hong Kong Baptist University, Hong Kong SAR, China  
E-mail: {ymc, cszhk, cswclan}@comp.hkbu.edu.hk

Hui Huang  
College of Computer Science and Software Engineering, Shenzhen University, China  
E-mail: huihuang@szu.edu.cn

\*Yiu-ming Cheung is the corresponding author.

spaces of all classes can be calibrated. In such balanced-distributed embedding spaces, the biased classifier can be eliminated by simply retraining the classifier with class-balanced sampling data. Extensive experiments conducted on benchmark datasets demonstrate the superior performance of the proposed method over the state-of-the-art ones.

**Keywords** Imbalance learning · long-tailed classification · Gaussian clouded logit · logit adjustment

## 1 Introduction

DEEP learning methods have achieved better-than-human performance on a variety of visual recognition tasks (He et al., 2016; Wang et al., 2017a; Jiangmiao et al., 2021) by virtue of the large-scale annotated datasets. In general, the success of deep neural networks (DNNs) relies on balanced-distributed data and sufficient training samples. That is, the number of samples in each class is basically the same and large enough. Unfortunately, from the practical perspective, data collected from the real world would follow a power-law distribution (Kendall et al., 1948; Clauset et al., 2009), which means that a tiny number of head classes occupy large volumes of instances while the vast majority of tail classes each have fairly few samples, showing a “long tail” in the data distribution. In fact, class importance is independent of the number of training samples. In other words, few samples cannot imply the unimportance of the tail classes (Yang et al., 2022; Zang et al., 2023). Even more, misclassification of tail classes can have severe consequences, especially in critical applications such as medical diagnosis or road monitoring. Therefore, it is important to develop methods that can effectively address the long-tailed distribution of data and improve the recognition performance on tail classes particularly.

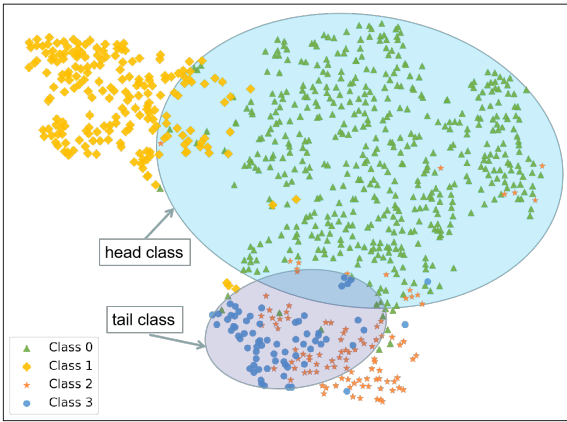


Fig. 1: T-SNE visualization of the distorted embedding space<sup>1</sup>. The embedding distributions of head and tail classes are shown in shaded areas. We can see that there are many overlapping regions between each class.

In the literature, many researchers have addressed the issue of long-tailed visual recognition by focusing on the classifier level. It is well-known that DNN can be decoupled into a feature extractor and a classifier (Huang et al., 2022; Du et al., 2021; Li and Huang, 2022; Chen et al., 2022). Recently, Zhou et al. (Zhou et al., 2020) have conducted empirical studies to demonstrate that the features (also referred to as *embeddings* interchangeably hereinafter) obtained from the original long-tailed dataset are already sufficiently representative. Consequently, they shifted their focus to balancing the classifier through two versions of sampling data. Also, two-stage decoupling methods (Kang et al., 2020; Cao et al., 2019; Wang et al., 2020a; Zhang et al., 2021a) have been proposed to obtain a representation in the first stage and then re-train the classifier on balanced sampling data in the second stage. These methods obtain the representation by cross-entropy (CE) loss, which, however, leads to a severely uneven distribution of the embedding space, hindering the acquisition of a better classifier. Furthermore, re-training the classifier can only alleviate the classifier bias but cannot adjust the distorted embedding space, which is not conducive to further promoting the model performance.

For the feature issue, specifically, the embedding spatial span of tail classes is drastically compressed by head classes because they have limited training samples that cannot cover the true distribution in embedding space. For ease of understanding, we use a simple experiment to demonstrate the distortion of the embedding space, as illustrated in Fig. 1, where the features are projected by t-SNE (Van der Maaten

<sup>1</sup> The embeddings are obtained by CE loss from a subset with four classes in CIFAR-10-LT. We randomly select 500, 200, 100, and 50 samples for each class to simulate the data imbalance.

and Hinton, 2008). It can be observed that the tail class occupies a much smaller spatial span than the head class.

A straightforward way to calibrate the distorted embedding space is to enlarge the spatial distribution of tail classes. Analogous to human cognition, where a person is capable of inferring the extension of an entire category from a single instance (Smith and Sloane, 2017), we treat one training sample as a set of similar samples. By augmenting the features, we can control the spatial span of the embedding. As only the orientation of the class anchors contributes to the classification, we increase the perturbation amplitude of the tail classes along the direction of the corresponding class anchors. This expands the spatial distribution of tail classes and prevents them from being overly compressed by head classes. Conversely, these amplitudes for head classes should be small. Since their samples with enough diversity already cover the actual spacial span, additional expansion is no need anymore. Eventually, as shown in Fig. 2, the tail class samples can be pushed further away from the other classes so that the distortion of the embedding space can be well calibrated. To this end, we first expand the embedding spatial span with a Gaussian form of perturbation. Based on this, we propose a novel logit adjustment method in two forms: normalized Euclidean and Angular. This method improves model performance with negligible additional computation. Since Gaussian distribution has a cloud-like shape, we name the perturbation amplitude as cloud size and the proposed method as Gaussian clouded logit (GCL). After calibrating the embedding space with GCL, the features of different classes can be more evenly distributed. It turns out that the classifier bias can be easily eliminated through class-balanced sampling data (Cui et al., 2019; Huang et al., 2016; Wang et al., 2017b; Mahajan et al., 2018; Cui et al., 2018) in such a balanced-distributed space. Extensive comparison experiments implemented on multiple commonly used long-tailed benchmarks demonstrate the superiority of the proposed GCL.

Compared to our preliminary work reported in (Li et al., 2022a), the main difference of this paper is as follows: Firstly, this paper provides a general form of perturbed logit by perturbing the logit to calibrate the distribution of embedding space. Accordingly, two specific forms based on different metrics are derived from this general form. Secondly, we present the analysis and explanation of the rationale of GCL in detail, based on which more general parameter selection strategies are provided. After calibrating the embedding space with GCL, the classifier bias can be mitigated by simply retraining with the balanced sampling data. Thirdly, more experiments are conducted to demonstrate the effectiveness of the proposed method. Specifically, we add more classification baselines to show the efficacy of GCL. Furthermore, we demonstrate that GCL can enhance the performance of mixture of experts (MoE)

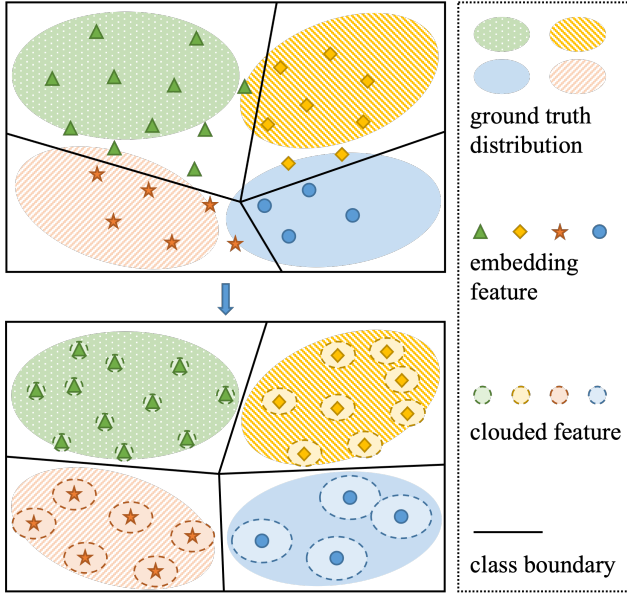


Fig. 2: Overview of the proposed method. The embedding distribution obtained by CE loss is uneven, leading to difficulty in classifying the tail class. By assigning larger cloud sizes to the tail class features, the distortion of the embedding space can be well calibrated.

model. Additionally, we provide in-depth theoretical and experimental analyses of the characteristics of GCL in both its normalized Euclidean and angular forms.

In summary, the main contributions of this paper are three-fold:

- We propose a simple but effective GCL adjustment method derived from the Gaussian perturbed feature. Tail classes are assigned larger cloud sizes than head classes along the direction of the corresponding class anchors. Consequently, it can address the problem of the distorted embedding space caused by long-tailed data.
- We provide in-depth discussions into GCL for long-tail learning from the perspective of optimization and geometric interpretation. They help set the sign and magnitude of the perturbation and provide a new idea for better generalization to test set.
- We obtain two specific forms of GCL. Both of them outperform the state-of-the-art counterparts on long-tailed benchmark datasets without additional computation. Their advantages and disadvantages in different long-tailed scenarios are analyzed in detail.

The remainder of this paper is organized as follows. Section 2 makes an overview of the recent related works. Section 3 details the derivation and rational analysis behind the proposed Gaussian clouded logit. Section 4 presents our experimental results in comparison with the baseline

methods, as well as model validation and analysis. Finally, Section 5 draws a conclusion.

## 2 Related Works

Over the past years, a number of methods have been proposed to address long-tailed visual recognition. This section makes an overview of the most related four regimes. That is, data augmentation, two-stage method, mixture of experts, and loss modification and logit adjustment.

### 2.1 Data Augmentation

Input augmentation increases sample diversity in the data space. The classical augmentation methods (He et al., 2016; Szegedy et al., 2015) include flip, rotate, crop and padding etc. Most recently, Wang et al. (Wang et al., 2021a) have proposed rare-class sample generator (RSG) that augments the minority classes via the encoded variation information obtained from frequent classes. Differently, M2m (Kim et al., 2020) constructs a balanced dataset by translating head class samples to the tail classes via an auxiliary pre-trained classifier.

Feature augmentation augments data diversity in feature space. Knowledge transfer is a promising technology. For instance, Yin et al. (Yin et al., 2019) transferred the intra-class variance of head classes obtained from an encoder-decoder based network to augment the feature of tail class samples. Liu et al. (Liu et al., 2020) transferred the angular variance calculated from head classes to tail classes to enrich the intra-class diversity of tail classes. Furthermore, class activation maps (CAM) (Zhou et al., 2016) have been adopted in long-tailed data recently. Chu et al. (Chu et al., 2020) utilized CAM to decompose the features into a class-generic and a class-specific component. Then, tail classes are augmented by fusing the class-specific components obtained from the tail classes with the class-generic components of the head classes. Also, Zhang et al. (Zhang et al., 2021b) exploited CAM to obtain the foreground in an image and then augment the obtained foreground object by flipping, rotating, jittering, etc. The augmented foreground is then covered on the unchanged background to obtain a new informative image.

Those methods mentioned above require either an increase in data size or model complexity to solve the issues in long-tailed distribution, resulting in additional computational costs.

### 2.2 Two-stage Method

Recently, two-stage methods have been proposed and experimentally shown their effectiveness. For example, Cao

et al. (Cao et al., 2019) proposed LDAM-DRW, learning features in the first stage and adopting a deferred re-weighting (DRW) strategy to fine-tune the classifier in the second stage. It significantly improves the long-tailed prediction accuracy, but the theoretical explanation of DRW is unclear. After that, Kang et al. (Kang et al., 2020) precisely pointed out that the learning process of representation and classifier can be decoupled into two separate stages. The first stage performs representation learning on the original long-tail data. The second stage fixes the parameters of the backbone network and re-trains the classifier with class-balanced sampling data. A number of works (Wang et al., 2020a; Zhang et al., 2021a; Wang et al., 2020b; Zhong et al., 2021) have further refined this strategy. For example, Zhang et al. (Zhang et al., 2021a) proposed an adaptive calibration function to calibrate the predicted logits of different classes into a balanced class prior to the second stage. Zhong et al. (Zhong et al., 2021) proposed class-based soft label to cope with different degrees of overconfidence in the predicted logit of each class, which can improve the classifier learning in the second stage. Another alternative is proposed by Zhou et al. (Zhou et al., 2020), which splits the network structure into two branches. One of the branches focuses on learning the representation of head and the other is for tail classes. This structure incorporates feature mixup (Verma et al., 2019) into a cumulative learning strategy and achieves state-of-the-art results. Thereafter, Wang et al. (Wang et al., 2021b) introduced contrastive learning into this bilateral-branch structure, further enhancing the long-tailed classification performance.

### 2.3 Mixture of Experts

More recently, researchers have explored the use of mixture of experts (MoE) methods to enhance performance by integrating multiple models into the learning framework. The fundamental concept behind these approaches is to introduce diversity to the data or models, which enables experts to concentrate on different portions of the data or allows experts with different structures to analyze the data. BBN (Zhou et al., 2020) proposes a two-branched classifier that learns both the long-tailed and inverse distributions simultaneously, with a smooth transition of focus between them. BAGS (Li et al., 2020), LFME (Xiang et al., 2020), and ACE (Cai et al., 2021) divide the long-tailed data into different sub-splits and fit multiple experts on them. ResLT (Cui et al., 2023) designs residual structured classifiers that allow experts to specialize in different parts of the long-tailed data and complement each other. RIDE (Wang et al., 2021c) and TLC (Li et al., 2022b) employ multiple experts, each trained on different augmented data, to independently learn the long-tailed distribution. The predictions of all experts are then gradually integrated to reduce

overall model variance or uncertainty. SHIKE (Jin et al., 2023) investigates the impact of feature depth on data of varying scales in long-tailed visual recognition. The authors propose a new architecture, which incorporates features from different layers of a neural network to exploit the rich information present at different depths of a network. NCL Li et al. (2022c) adopts multiple complete networks to learn the long-tailed data individually and uses self-supervised contrastive strategy Cui et al. (2021) to collaboratively transfer knowledge among each individual expert.

### 2.4 Loss Modification and Logit Adjustment

Re-weighting the loss function is one of the most intuitive ways to improve the attention of DNN model on tail classes. In the literature, sample-wise re-weighting (Ren et al., 2018; Lin et al., 2020) introduces the fine-grained coefficients into the loss function to make the model pay more attention to the difficult samples. Furthermore, class-wise re-weighting (Cui et al., 2019; Huang et al., 2016; Khan et al., 2018; Tan et al., 2020; Sinha et al., 2022) assigns the standard CE loss with category-specific parameters that are inversely proportional to the class sizes. These methods can alleviate the data imbalance to a certain extent. However, when the imbalance ratio is very high, large weights may cause overfitting to the tail classes. Besides that, another side effect of assigning higher weights to difficult samples/tail classes is overly focusing on harmful samples (e.g., abnormal samples or mislabeled data) (Koh and Liang, 2017).

Loss function can also be modified by adjusting the logit. Menon et al. (Menon et al., 2021) proposed logit adjustment (LA), which is consistent in minimizing the balanced error. The logit shifting in LA of different classes is based on label frequencies of training data. By contrast, LADE (Hong et al., 2021) post-processes the model prediction by disentangling the training set distribution from the prediction. This method does not require the test set to be a uniform distribution. Also, DisAlign (Zhang et al., 2021a) adjusts the logit by calibrating the distribution of model prediction to a balanced one by minimizing the expected KL divergence. Overall speaking, these three methods can well adjust the classifier but do not take into account the distorted embedding space. Alternatively, re-margining methods (Cao et al., 2019, 2020; Li et al., 2023) address long-tailed data by leaving large relative margins for tail classes during training. For example, label-distribution-aware margin (LDAM) loss (Cao et al., 2019) utilizes Rademacher complexity to theoretically prove that the margin should be inversely proportional to a quarter power of class sizes. The hard margin on target logit helps make the samples within a class more compact but the strict margin constraints increase the risk of overfitting and cannot actually expand the tail class coverage area in embedding space.

### 3 Proposed Method

The basic idea of our proposed method is to perturb the features with varying magnitudes in the directions of different class anchors, thereby automatically balancing the spatial span of head and tail classes. The details of the proposed approach are presented as follows.

#### 3.1 Basic Notations

This section defines the notation used throughout this paper.

##### 3.1.1 For dataset

Suppose  $\{x, y\} \in \mathcal{T}$  represents a sample  $\{x, y\}$  from the training set  $\mathcal{T}$ , where  $\mathcal{T}$  has  $C$  classes and  $N$  training samples in total,  $x$  represents the image that needs to be classified and  $y \in \{1, \dots, C\}$  is the ground truth label. The number of training samples of class  $j$ , ( $j = \{1, 2, \dots, C\}$ ) is  $n_j$  and  $\sum_{j=1}^C n_j = N$ .

##### 3.1.2 For backbone

$\mathbf{f} \in \mathbb{R}^D$  is the feature obtained from the embedding layer, and the dimension is  $D$ .  $\mathbf{W} = \{\mathbf{w}_1, \mathbf{w}_2, \dots, \mathbf{w}_C\} \in \mathbb{R}^{D \times C}$  represents the weight matrix of the classifier, where  $\mathbf{w}_j$  represents the anchor vector of class  $j$  in the classifier. The predicted logit of class  $j$  is represented by  $z_j$ , thus,  $z_j = \mathbf{w}_j^T \mathbf{f}$ . The subscript  $y$  indicates the target class. That is,  $z_y$  denotes the target logit and  $z_j, j \neq y$  is the non-target logit.

#### 3.2 Embedding Space Calibration

Suppose a feature point and a small area around it belong to the same type. It is reasonable that the adjacent points around a feature can be regarded as similar to it, and can naturally be considered as the same class.

##### 3.2.1 General form via perturbing the embedding representation

We sample a set of points by adding perturbations following a specific distribution to a given feature. Then, a perturbed feature  $\mathbf{f}^{ptb}$  of the input is represented as:

$$\mathbf{f}^{ptb} \triangleq \mathbf{f} + \delta \mathbf{E}, \quad (1)$$

where  $\mathbf{E}$  represents the perturbation and  $\delta > 0$  is the amplitude of it. To avoid misleading the final classification, the perturbation amplitude cannot be too large, thus  $\delta$  should be a small number. This perturbed feature is the input of

the classifier. Then, the corresponding perturbed logit  $z_j^{ptb}$  of class  $j$  is calculated by:

$$\begin{aligned} z_j^{ptb} &= \mathbf{w}_j^T \mathbf{f}^{ptb} + \mathbf{b}_j \\ &= \mathbf{w}_j^T \mathbf{f} + \mathbf{b}_j + \mathbf{w}_j^T (\delta \mathbf{E}) \\ &= z_j + \delta (\mathbf{w}_j^T \mathbf{E}), \end{aligned} \quad (2)$$

where  $z_j^{ptb}$  is the original logit  $z_j$  adding a perturbing item  $\delta (\mathbf{w}_j^T \mathbf{E})$ .

##### 3.2.2 Normalized Euclidean form

It should be noted that the perturbing item has different degrees of influence on the final predicted results based on different predicted logits. It has a relatively small impact on  $z_j^{ptb}$  when the original logit  $z_j$  is large. On the contrary, it will play a primary role for  $z_j^{ptb}$  when  $z_j$  is small. Therefore, we need to normalize the effect caused by different predicted logits and maintain the consistency of the influence of the perturbing item. Inspired by (Wang et al., 2017a, 2018; Deng et al., 2019), we use the cosine distance by normalizing the perturbed logits. In this way, the norm of the embedding and the class anchor will be normalized to constants. We use  $s_e$  and  $s_a$  to represent these two numbers. The normalized perturbed logit  $\tilde{z}_j^{ptb}$  is calculated by:

$$\begin{aligned} \tilde{z}_j^{ptb} &= \frac{s_a \mathbf{w}_j^T \cdot s_e \mathbf{f}^{ptb}}{\|\mathbf{w}_j^T\| \|\mathbf{f}^{ptb}\|} \\ &= s \cdot \left( \frac{\mathbf{w}_j^T \mathbf{f}}{\|\mathbf{w}_j^T\| \|\mathbf{f} + \delta \mathbf{E}\|} + \delta \frac{\mathbf{w}_j^T \mathbf{E}}{\|\mathbf{w}_j^T\| \|\mathbf{f} + \delta \mathbf{E}\|} \right), \end{aligned} \quad (3)$$

where  $s = s_e \cdot s_a$  is a constant.  $\|\mathbf{f} + \delta \mathbf{E}\|$  is approximate to  $\|\mathbf{f}\|$  because  $\delta$  is a small number. For the second term, we use  $\mathbf{I}_j$  to represent the identity vector that has the same direction as  $\mathbf{w}_j^T$ , namely  $\mathbf{I}_j = \frac{\mathbf{w}_j^T}{\|\mathbf{w}_j^T\|}$ . Eq. 3 is simplified as:

$$\begin{aligned} \tilde{z}_j^{ptb} &\approx s \cdot \left( \frac{\mathbf{w}_j^T \mathbf{f}}{\|\mathbf{w}_j^T\| \|\mathbf{f}\|} + \frac{\delta}{s_a} \mathbf{I}_j \mathbf{E} \right) \\ &= s \cdot \left( \cos \theta_j + \frac{\delta}{s_a} \mathbf{I}_j \mathbf{E} \right), \end{aligned} \quad (4)$$

where  $\theta_j$  is the angle between  $\mathbf{f}$  and  $\mathbf{w}_j$ . As additive Gaussian noise is a commonly used in machine learning (Vincent et al., 2008; Nazaré et al., 2018; Kim et al., 2019) because of the simplicity (MDixon and Massey Jr., 1951; Ott and Longnecker, 2015) and universality (Rasmussen, 1999; Mendenhall et al., 2013) of Gaussian distribution, in order to simplify the calculation, we also set the perturbation as Gaussian distribution, i.e.  $\mathbf{E} \sim \mathcal{N}(\mathbf{M}, \Sigma)$  where  $\mathbf{M} \in \mathbb{R}^D$  and  $\Sigma \in \mathbb{R}^{D \times D}$ . Further, we set  $\Sigma = \sigma \mathbf{I}$  where  $\mathbf{I} \in \mathbb{R}^{D \times D}$  is the identity matrix. Then  $\mathbf{I}_j \mathbf{E}$  is the projection of the perturbation on the direction of the anchor vector of class  $j$ . We direct use  $\varepsilon_j$  to represent this value, which

can be viewed as the projection amplitude. Taking it into Eq. 4 and uniformly shifting the class-related variable to the previously defined perturbation amplitude  $\delta$  for simplicity, we can get a more concise expression for  $\tilde{z}_j^{ptb}$ :

$$\begin{aligned}\tilde{z}_j^{ptb} &= s \cdot (\cos \theta_j + \frac{\delta}{s_a} \varepsilon_j) \\ &\Leftrightarrow s \cdot (\cos \theta_j + \delta_j \varepsilon).\end{aligned}\quad (5)$$

Since  $\varepsilon$  is also distributed in Gaussian form, it has a cloud-like shape.  $\delta_j$  is the class-based perturbation amplitude that depends on label frequencies. we name  $\delta_j$  cloud size because it controls the amplitude of  $\varepsilon$ . To broaden the embedding space for the tail classes, the cloud size for tail classes is required to be larger than that of the head classes. Therefore,  $\delta_j$  is negatively correlated with  $n_j$ .

As  $\varepsilon$  makes the logit has a cloud-like shape, we name the perturbed logit as *Gaussian clouded logit* (GCL). We delve into Eq. 5. If  $\varepsilon > 0$ ,  $\tilde{z}_j^{ptb}$  corresponds to the points that are closer to the anchor vector of class  $j$ . Those points can be classified correctly does not mean that the distant points of the same class can also be classified correctly, thus  $\varepsilon > 0$  will not be helpful for classification. On the contrary, a reduced logit corresponds to the points that are relatively far from the class anchor. If the relatively distant points can be predicted correctly, the closer one will definitely be able to assign the right label. The points in the same class that are relatively far from the class anchor should be focused on.  $\varepsilon$  therefore should always be negative. We name this logit as GCL in normalized Euclidean form (GCL-E for short) because it is derived from normalized Euclidean distance metric. We modify the perturbed logit and use  $\tilde{z}_j^{GCL-E}$  to represent it, which is expressed as:

$$\tilde{z}_j^{GCL-E} = s \cdot (\cos \theta_j - \delta_j \|\varepsilon\|). \quad (6)$$

### 3.2.3 Angular form

The final logit of GCL in normalized Euclidean form is equivalent to adding a class-based perturbation on cosine logit. From another perspective, namely metric learning, Eq. 6 corresponds to adding a Gaussian form margin with class-based variance to the cosine logit (Section 3.2.4 provides a detailed analysis). Inspired by Deng et al. (Deng et al., 2019), this Gaussian form margin can also be introduced into the angular distance metric. For the sake of distinguishing from GCL-E, this version of GCL is named GCL in Angular form (GCL-A for short). Use  $\tilde{z}_j^{GCL-A}$  to represent, then, GCL-A for class  $j$  can be calculated by:

$$\tilde{z}_j^{GCL-A} = s \cdot \cos(\theta_j + \delta_j \|\varepsilon\|), \quad (7)$$

where  $\theta_j + \delta_j \|\varepsilon\|$  corresponds to the relatively distant points in the same class, so Eq. 7 is consistent with Eq. 6.

By taking the Gaussian clouded logit into the original softmax, we obtain the final loss function of GCL:

$$\mathcal{L}_{GCL}^* = -\frac{1}{N} \sum_i \log \frac{e^{\tilde{z}_i^{GCL}}}{\sum_j e^{\tilde{z}_j^{GCL}}}, \quad (8)$$

where  $\tilde{z}_j^{GCL}$  can be the logit of GCL-E ( $\tilde{z}_j^{GCL-E}$ ) or GCL-A ( $\tilde{z}_j^{GCL-A}$ ).  $\mathcal{L}_{GCL-E}$  is utilized to represent the loss function of GCL-E and  $\mathcal{L}_{GCL-A}$  denotes that of GCL-A.

### 3.2.4 Rationale Analysis

This sub-section provides a detailed rationale analysis of how Eq. 6 and Eq. 7 can balance the embedding space from two perspectives, i.e. model optimization and metric learning.

**The Perspective of Model Optimization** In backward propagation, the gradients on logit  $z_i$  are calculated by:

$$\frac{\partial \mathcal{L}}{\partial z_i} = \begin{cases} p_i - 1, & i = y \\ p_i, & i \neq y \end{cases}, \quad (9)$$

where  $p_i = \frac{e^{z_i}}{\sum_{j=1}^C e^{z_j}}$ . We take the binary case to illustrate without loss of generality. Suppose the input image is from class 1. The gradient on  $z_1$  is calculated by:

$$\frac{\partial \mathcal{L}}{\partial z_1} = -\frac{1}{1 + e^{z_1 - z_2}}. \quad (10)$$

Eq. 10 indicates that the gradient of the target class rapidly approaches zero with the increase of the target logit. This phenomenon is called softmax saturation (Chen et al., 2017; Zhang et al., 2021c). This inopportune early gradient vanishing weakens the validity of training samples and impedes model training. Therefore, softmax can only slightly separate various classes, and lacks the impetus to evenly distribute each class in the embedded space. We can also observe that there are many overlapping areas among each class in Fig. 1. Especially under the circumstances of long-tailed classification, the tail class features are insufficient to cover the ground truth distribution in embedding space. The early gradient vanish caused by soft saturation exacerbates the squeezing of the embedding distribution in tail class.

Different from the original softmax loss function, the logit difference ( $\Delta_{y-j}$ ) obtained by GCL of Eq. 6 between the target and non-target classes is calculated by:

$$\begin{aligned}\Delta_{y-j} &= \tilde{z}_y^{GCL-E} - \tilde{z}_j^{GCL-E} \\ &= s \cdot (\cos \theta_y - \cos \theta_j - (\delta_y - \delta_j) \|\varepsilon\|).\end{aligned}\quad (11)$$

In case the target class is a tail class,  $\delta_y - \delta_j > 0$ , which decreases the softmax saturation and thereby helps increase the validity of tail class samples. Eq. 7 has the same effect. Thus, Eq. 6 and Eq. 7 can automatically balance the sample

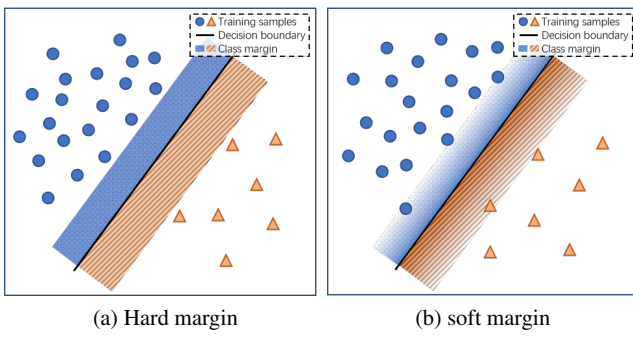


Fig. 3: Schematic comparison of hard margin and soft margin. The blue dots and pink triangles represent the head and tail classes, respectively. (Color for the best view.) (a) The hard margin strictly restricts samples from appearing in the corresponding region. (b) The soft margin allows outliers to appear in the region with a lower probability, which increases generalization.

validity of different classes and provide incentives for the model to make each class more separable. They achieve the aim of calibrating the distorted embedding space.

**The Perspective of Metric Learning** Compared with the prior work that enlarges the inter-class separability via the “hard margin”, e.g. see (Cao et al., 2019; Deng et al., 2019; Zhang et al., 2021c), Eq. 6 and Eq. 7 are equivalent to adding a “soft” margin. That is, the farther away from the class anchor, the lower the probability that the point belongs to this class. Fig. 3 schematically shows the comparison of the prior hard margin and the proposed soft margin. Hard margins will cause the samples to shrink toward the class anchor if the margin is too large. In addition to this, hard margins can lead to overfitting because it prohibits outliers, which can impair the robustness ability of the model. The proposed soft margin provides a smooth transition area, allowing the outliers to appear near the target class with a lower probability. This is both intuitively and theoretically more reasonable.

The cloud size  $\delta_j^*$  may also take different expression forms, where the superscript \* indicates the adopted specific form. Cao et al. (Cao et al., 2019) obtained the optimal trade-off of the hard margin ( $m_i$ ) and the class size via Rademacher complexity. They have proved that  $m_i \propto n_i^{-1/4}$ . The exponent should be  $-1/3$  derived from Wei et al. (Wei and Ma, 2020). Inspired by these works, we can set the cloud size in power function form:

$$\delta_j^{pow} = n_{max} \cdot n_j^{-k}, \quad (12)$$

where  $n_{max}$  is the sample number of the most frequent class.  $k$  can be  $1/3$  or  $1/4$ . Menon et al. (Menon et al., 2021) used the Fisher consistency with respect to the balanced error and

obtained that  $m_i \propto \log(1/n_j)$ . Therefore, we can also set the cloud size in logarithmic form:

$$\delta_j^{log} = \log n_{max} - \log n_j. \quad (13)$$

We also experimentally demonstrate the effectiveness of the cloud size in different expression forms in Section 4.5.3.

In short, GCL in the form of either normalized Euclidean distance or angular distance can achieve the following three advantages: 1) reduce the softmax saturation and thereby increase the sample validity of tail classes; 2) avoid overfitting and improve robustness through randomly sampling the values in Gaussian distribution. 3) enlarge the margin of class boundary for tail classes and thus can calibrate the distortion of the embedding space. The slight difference between the two forms is that GCL-E is to add the class-based perturbation on features before the calculation of logit, while GCL-A is equivalent to sampling disturbed feature points after knowing the distance from the class anchor.

### 3.2.5 Time-complexity analysis

The softmax has a time complexity of  $\mathcal{O}(C)$ , which is linear with the dimension of logit. It is the same as cross-entropy loss  $\mathcal{L}_{CE}$  and  $\mathcal{L}_{GCL}$  in both forms. The main difference in time complexity comes from the calculation of logit. For the original normalized logit (which is denoted as  $\tilde{z}_j = s \cdot \cos \theta_j$ ), its main computational cost is vector multiplication. It contains  $D \cdot C$  multiplications and  $(D - 1) \cdot C$  additions. Thus, the time complexity of computing  $\tilde{z}_j$  is  $\mathcal{O}(DC)$ . Eq. 6 shows that GCL-E only adds  $C$  scalar additions to  $\tilde{z}_j$ . As a result, computing  $\tilde{z}_j^{GCL-E}$  has  $\mathcal{O}(DC)$  time-complexity. For GCL-A, we first expand Eq. 7 to  $\tilde{z}_j^{GCL-A} = s \cdot (\cos \theta_j \cos \delta_j \|\varepsilon\| - \sin \theta_j \sin \delta_j \|\varepsilon\|)$ . The sine value can be obtained from the corresponding cosine value. Compared to  $\tilde{z}_j$ , GCL-A adds an additional  $2C$  multiplications and  $C$  subtractions. Computing  $\tilde{z}_j^{GCL-A}$  also has  $\mathcal{O}(DC)$  time-complexity. It is obvious that GCL in both forms imposes a negligible additional burden on the training process.

### 3.3 Classifier Re-balance

Although both GCL-E and GCL-A calibrate the distorted embedding space well, the problem of classifier bias still remains to be addressed.

In the following, we analyze the reasons for the biased classifier. Eq. 9 implies that the sample of the target class  $y$  punishes the classifier weights  $\mathbf{w}_j$  of non-target class  $j, j \neq y$  w.r.t.  $p_j$ . In general, the number of training instances in head classes is enormously greater than in tail classes. Therefore, the classifier weights of tail classes receive much more penalty than positive signals during training. Consequently, the classifier will bias towards the head classes

**Algorithm 1:** GCL with cRT

---

```

Input: Training dataset  $\mathcal{T}$ ;
Output: Predicted labels;
1 Initialize the model parameters  $\omega$  of the backbone network
 $\phi((x,y); \omega)$  randomly ;
2 for  $iteration = 1$  to  $I_0$  do
3   Sample a batch data  $\mathcal{B}$  from the original long-tailed
   dataset  $\mathcal{T}$  with a batch size of  $b$ ;
4   Calculate the logit cloud size  $\delta_j$  by Eq. 12 (or Eq. 13):
 $\delta_j \leftarrow n_{max} \cdot n_j^{-k}$  (or  $\delta_j \leftarrow \log n_{max} - \log n_j$ );
5   Calculate the loss by Eq. 8:
 $\mathcal{L}((x,y); \omega) = \frac{1}{b} \sum_{(x,y) \in \mathcal{B}} \mathcal{L}_{GCL}^*(x,y);$ 
6   Update model parameters:
 $\omega = \omega - \alpha \nabla_{\omega} \mathcal{L}((x,y); \omega).$ 
7 end
8 for  $iteration = I_0 + 1$  to  $I_0 + I_1$  do
9   Calculate sampling rate by Eq. 14 (or Eq. 15):
 $q_j \leftarrow n_j / \sum n_j$  (or  $q_j \leftarrow n_j^{en} / \sum n_j^{en}$ );
10  Sample a batch data  $\mathcal{B}'$  with the sampling rate  $q_j$  and the
    batch size  $b$ ;
11  Calculate the loss by Eq. 8:
 $\mathcal{L}((x,y); \omega) = \frac{1}{b} \sum_{(x,y) \in \mathcal{B}'} \mathcal{L}_{GCL}(x,y);$ 
12  Update classifier parameters  $\omega_{cls}$  (representation
    parameters are frozen):
 $\omega_{cls} = \omega_{cls} - \alpha \nabla_{\omega_{cls}} \mathcal{L}((x,y); \omega_{cls}).$ 
13 end

```

---

and the predicted logits of the tail classes will be seriously suppressed, resulting in low classification accuracy of the tail classes (Tan et al., 2020; Wang et al., 2021d,e). We call this problem of the cross-entropy loss function in long-tailed learning *negative gradient over-suppression*. A straightforward approach to cope with it is to make the sample numbers of each class equal to balance the negative gradients. To achieve this goal, we can make the tail classes over-sampling and then re-train the classifier. The sampling rate of each class is  $\frac{1}{C}$ . Then, the class-balanced sampling rate  $q_j^{cb}$  of each sample  $x$  from class  $j$  is calculated by:

$$q_j^{cb} = \frac{1}{C \cdot n_j}. \quad (14)$$

This strategy is called classifier re-training (cRT) (Kang et al., 2020). It can also be combined with the *effective number* (Cui et al., 2019). We can replace the actual sample number  $n_j$  of class  $j$  with the so-called *effective number*  $n_j^{en}$ , the effective sampling rate  $q_j^{en}$  of each sample from class  $j$  is given by:

$$q_j^{en} = \frac{1}{C \cdot n_j^{en}}, \quad (15)$$

where  $n_j^{en}$  is calculated by:

$$n_j^{en} = \frac{1 - \beta^{n_j}}{1 - \beta} N, \quad (16)$$

with hyper-parameter  $\beta \in [0, 1)$ . Algorithm 1 summarizes the overall training procedure of the proposed method.

**4 Experiments**

This section first introduces five long-tailed datasets used in our experiments in Section 4.1. Then, the detailed implementation settings of the experiments are presented in Section 4.2. To demonstrate the effectiveness of GCL, we compare the proposed two forms of GCL with state-of-the-art methods based on a single model structure. The classification accuracy is compared in Section 4.3. Moreover, Section 4.4 validates that GCL can also enhance the performance of MoE model. Finally, the model validation experiments and ablation studies are conducted to show the properties of our proposed method in Section 4.5.

**4.1 Benchmark Datasets**

We use five benchmarks: CIFAR-10-LT and CIFAR-100-LT, ImageNet-LT, iNaturalist 2018, and Places-LT.

**CIFAR-10/100-LT** The original versions of CIFAR-10 and CIFAR-100 (Krizhevsky et al., 2009) are uniformly distributed datasets, which consist of 10 and 100 classes, respectively. They both contain 60K images with a size of  $32 \times 32$ . The training set contains 50K samples and the test set has 10K samples. Following the experimental settings in (Cao et al., 2019; Cui et al., 2019), we down-sampling training images per class with the exponential function  $n_i = n_i^o \times \lambda^i$ , where  $i$  is the class index (0-indexed),  $n_i^o$  is the label frequency in the original balanced version and  $\lambda \in (0, 1)$ . The test sets are kept unchanged. The imbalance ratio  $r$  is defined as the ratio of the maximum and minimum label frequencies, i.e.,  $r = \max(n_i) / \min(n_i), i = 1, 2, \dots, C$ . We adopt the most widely used three imbalance ratios, i.e.,  $r = 50, 100$ , and 200 in the comparison experiments.

**ImageNet-LT and Places-LT** The original versions of ImageNet (Russakovsky et al., 2015) and Places (Zhou et al., 2017) are artificially balanced, large-scale real-world datasets for classification and localization. We follow Liu et al.’s (Liu et al., 2019) setting to construct the long-tailed version of these two datasets by truncating a subset with the Pareto distribution with the power value  $\alpha = 6$  from the balanced versions. The original validation sets are used for testing. Overall, ImageNet-LT includes 115.8K training images from 1K categories with  $r = 1,280/5$ . Places-LT contains 62.5K training images from 365 categories with  $r = 4,980/5$ .

**iNaturalist 2018** iNaturalist 2018 (Van Horn et al., 2018) is a real-world fine-grained dataset for classification and detection, which is a naturally long-tailed distributed dataset. It contains different species of plants and animals collected from the real world in a wide variety of situations. This

dataset contains over 437.5K training samples and more than 24.4K validation images from 8,142 categories. The official validation set is utilized for testing in the experiments. The imbalance ratio of iNaturalist 2018 is  $r = 1,000/2$ .

## 4.2 Basic Setting

The parameters that need to be pre-set are the Gaussian distribution parameters  $(\mu, \sigma^2)$ . For GCL-E, the maximum cloud size cannot exceed 1 because  $\cos \theta_i \in [-1, 1]$ . Gaussian distribution has a probability of 99.7% falling in  $[\mu - 3\sigma, \mu + 3\sigma]$ , we therefore set  $\mu = 0$  and  $\sigma = \frac{1}{3}$ . We further clamp  $\varepsilon$  to  $[-1, 1]$  to prevent the cloud size from exceeding 1. For GCL-A, we first constrain the range of  $\varepsilon$  to  $[-1, 1]$  in the same way as the cosine form GCL. Then, we multiply  $\varepsilon$  with a constant  $\frac{\pi}{2}$  to limit the cloud size in angular form to  $[-\frac{\pi}{2}, \frac{\pi}{2}]$  based on the lemma<sup>2</sup> proposed by Ranjan et al. (Ranjan et al., 2017). Moreover, we normalize  $\delta_i$  by  $\delta_i \triangleq \delta_i / \max(\delta_i), i = 1, 2, \dots, C$  to ensure that maximum value of  $\delta_i$  does not exceed 1. For data augmentation techniques, we follow Zhong et al. (Zhong et al., 2021), except for basic augmentation such as image flip, rotation, and random crop, only mixup (Zhang et al., 2018) are adopted in all experiments to ensure fair comparisons.

PyTorch (Paszke et al., 2019) is utilized to implement the backbone network training. SGD optimizer with a momentum of 0.9 and the multi-step learning rate schedule is adopted. All the models are trained from scratch except ResNet-152 which is pre-trained on the original balanced version of ImageNet-2012. For the first stage, we select ResNet-32 as the backbone network and follow the experimental settings described in Cao et al. (Cao et al., 2019) for CIFAR-10/100-LT. For the experiments on large-scale datasets, namely, ImageNet-LT, iNatralist 2018, and Places-LT, we mainly follow Kang et al.’s settings (Kang et al., 2020) except for the learning rate schedule. For the second stage, i.e., re-balancing the classifier, we follow Kang et al.’s setting (Kang et al., 2020) for all datasets.

## 4.3 Main Comparison Results

### 4.3.1 Competing Methods

The competing methods include the following two groups:

**Baseline Methods** Vanilla training with cross-entropy (CE) loss is one of our baseline methods. Several visual recognition studies (Cao et al., 2019; Li et al., 2018; Hou et al.,

<sup>2</sup> **Lemma:** The classes can be distributed on a hyper-sphere of dimension  $D$  such that any two class centers (namely, class anchors in this paper) are at least  $\pi/2$  apart if the number of classes  $C$  is less than twice the feature dimension  $D$ .

2019; Wang and Deng, 2021) have demonstrated the efficacy of cosine similarity that can reduce the impact of imbalanced feature bias in imbalanced data distributions. Therefore, we also include CosFace (Wang et al., 2018) and ArcFace (Deng et al., 2019) as baseline methods.

**State-of-the-art Methods** We compare with the most recently proposed state-of-the-art methods including TSC (Li et al., 2022d), MBJ (Liu et al., 2022), FBL (Li et al., 2022e), and the two-stage methods including LDAM-DRW (Cao et al., 2019) and MisLAS (Zhong et al., 2021), which all achieve satisfactory classification accuracy on the aforementioned five long-tailed datasets. For a fair comparison, we implement the experiment of the two-stage strategy, i.e., adding mixup (Zhang et al., 2018) to decoupling (Kang et al., 2020) on all datasets. For CIFAR-10/100-LT datasets, we make a comparison with the logit adjustment method (De-confound-TDE (Tang et al., 2020)). BBN (Zhou et al., 2020) and contrastive learning (Wang et al., 2021b) are also included in the competing methods. For large-scale datasets, the representation learning method (OLTR (Liu et al., 2019)), and logit adjustment method (logit adjustment (Menon et al., 2021)) are included. The two-stage methods including decoupling (Kang et al., 2020), and DisAlign (Zhang et al., 2021a) are also compared.

### 4.3.2 Comparison Results

Extensive comparative experiments are conducted to illustrate the efficacy of our proposed GCL in two forms (GCL-E and GCL-A). The evaluation metric for assessing performance is top-1 accuracy on the test/validation sets. For comparison methods that have not released official code or relevant hyper-parameters, we quote the results directly from the original papers

**Experimental Results on CIFAR-10/100-LT** The proposed GCL-E and GCL-A both outperform the previous methods by notable margins with all imbalanced ratios. Especially for the largest  $r$ , i.e., 200, the proposed approach has obvious improvement. For example, GCL-E gets 79.03% and 44.84% in top-1 classification accuracy for CIFAR-10-LT and CIFAR-100-LT with  $r = 200$ , which surpasses the second-best method, i.e., FBL (Li et al., 2022e) (on CIFAR-10-LT) and MisLAS (Zhong et al., 2021) (on CIFAR-100-LT) by a significant margin of 0.93% and 2.51%, respectively. GCL-A further improves the performance compared to cosine form except on CIFAR-10-LT with  $r = 100$  (82.72% top-1 accuracy, which is still higher than the existing methods). For example, it increases the top-1 accuracy from 44.84% to 46.53% for CIFAR-100-LT with  $r = 200$  compared to the cosine form. The margin is more than 3% compared to MisLAS. Interestingly, we can observe

Table 1: Comparison results on CIFAR-10/100-LT w.r.t. Top-1 accuracy (%).

Dataset	CIFAR-10-LT			CIFAR-100-LT		
Backbone	ResNet-32					
Imbalance ratio	200	100	50	200	100	50
CE loss	65.68	70.70	74.81	34.84	38.43	43.9
CosFace (Wang et al., 2018)	66.22	72.08	77.40	35.36	39.21	43.11
ArcFace (Deng et al., 2019)	66.50	73.76	78.19	36.64	39.06	43.40
LDAM-DRW (Cao et al., 2019)	73.52	77.03	81.03	38.91	42.04	47.62
De-confound-TDE* (Tang et al., 2020)	-	80.60	83.60	-	44.15	50.31
Decoupling (Kang et al., 2020)	73.06	79.15	84.21	41.73	45.12	50.86
BBN (Zhou et al., 2020)	73.47	79.82	81.18	37.21	42.56	47.02
Contrastive learning (Wang et al., 2021b)	-	81.40	85.36	-	46.72	51.87
MisLAS (Zhong et al., 2021)	77.31	82.06	85.16	42.33	47.50	52.62
TSC* (Li et al., 2022d)	-	79.70	82.90	-	43.80	47.40
MBJ (Liu et al., 2022)	77.06	81.10	<b>85.45</b>	41.92	46.05	52.43
FBL (Li et al., 2022e)	78.10	82.46	84.30	40.67	45.22	50.65
GCL-E (Ours)	<b>79.03</b>	<u>82.73</u>	85.43	<b>44.84</b>	<b>48.69</b>	<b>53.51</b>
GCL-A (Ours)	<u>79.31</u>	<u>82.72</u>	<b>85.58</b>	<u>46.53</u>	<u>49.97</u>	<u>54.75</u>

**Note:** \* denotes that the results are quoted from the corresponding papers.

Other results are obtained by re-implementing with the official codes.

The best and the second-best results are shown in **underline bold** and **bold**, respectively.

Table 2: Comparison results on ImageNet-LT, iNaturalist 2018 and Places-LT w.r.t. Top-1 accuracy (%)

Dataset	ImageNet-LT	iNaturalist 2018	Places-LT
Backbone	ResNet-50	ResNet-50	ResNet-152
CE loss	44.51	63.80	27.13
CosFace (Wang et al., 2018)	44.95	72.08	27.19
ArcFace (Deng et al., 2019)	44.54	66.72	27.63
LDAM-DRW (Cao et al., 2019)	49.96	68.15	37.73
OLTR* (Liu et al., 2019)	-	-	35.90
Decoupling (Kang et al., 2020)	51.68	70.16	38.51
Logit adjustment* (Menon et al., 2021)	51.11	66.36	-
DisAlign* (Zhang et al., 2021a)	52.91	70.06	39.30
MisLAS (Zhong et al., 2021)	52.71	<b>71.57</b>	<b>40.36</b>
TSC* (Li et al., 2022d)	52.40	69.70	-
MBJ* (Liu et al., 2022)	52.10	70.00	38.10
FBL (Li et al., 2022e)	50.70	69.90	38.66
GCL-E (Ours)	<b>54.84</b>	<u>72.01</u>	<b>40.62</b>
GCL-A (Ours)	<u>55.12</u>	71.14	39.22

**Note:** The same as Table 1.

that CosFace (Wang et al., 2018) and ArcFace (Deng et al., 2019) perform well compared to CE loss, illustrating the efficacy of angular distance metric in long-tail learning. In comparison to LDAM-DRW (Cao et al., 2019) that is also based on angular distance metric, our proposed solution is still the clear winner. The performance gain is obtained by the smooth margin that can avoid overfitting and improve robustness. The clear performance gain compared to decoupling (Kang et al., 2020) demonstrates that calibrating the feature space via GCL is beneficial to

the subsequent classifier learning. The results on CIFAR-10/100-LT datasets are summarized in Table 1.

**Experimental Results on Large-scale Datasets** The results on large-scale long-tailed datasets including ImageNet-LT, iNaturalist 2018, and Places-LT are reported in Tab. 2. We observe that GCL-E is superior to the prior arts on all datasets. On ImageNet-LT, it achieves 54.84% top-1 accuracy, outperforming DisAlign (Zhang et al., 2021a) by a large margin at 1.97% and MisLAS (Zhong et al., 2021) at 2.77%, respectively. On iNaturalist 2018, the proposed

GCL-E achieves 72.01% top-1 accuracy, which outperforms the second-best method by 0.44%. On Place-LT, our method achieves 40.62% top-1 classification accuracy. Although the performance gain compared with MisLAS on iNaturalist 2018 and Place-LT is not as high as other datasets, our method does not require hyper-parameters searching for different datasets and thus is relatively easy to implement. GCL-A largely improves the performance on ImageNet-LT from 54.84% to 55.12%, but it slightly decreases the accuracy on iNaturalist 2018 and Places-LT. GCL-A achieves 71.14% top-1 classification accuracy on iNaturalist 2018, which is lower than MisLAS but still outperforms the other baseline methods by notable margins, showing the effectiveness of angular perturbation to balance the embedding space distribution. On Places-LT, it has a lower accuracy than MisLAS and DisAlign.

#### 4.4 Effectiveness on MoE model

We select RIDE (Wang et al., 2021c) as a representative of MoE Models. The reproduction of RIDE in our experiment follows the original settings, which utilize LDAM loss and DRW strategy. We employed three experts in our MoE model and adopted the mixup technique to ensure a fair comparison. MoE models have been shown to outperform single models, albeit at the expense of increasing model size. For instance, RIDE with GCL-E achieved an accuracy of 81.32% on CIFAR-10-LT with an imbalance ratio of 200, which is an obvious improvement from the 79.03% achieved by a single ResNet-32 model with GCL-E. However, the model size of RIDE is 5.38 Mb, whereas the single model had a size of only 1.84 Mb. Tables 3 and 4 demonstrate the improvement in performance achieved by GCL on RIDE. Both versions of GCL can be observed to improve RIDE’s performance significantly on all dataset. The improvement of GCL-A ranges from 0.90% to 2.62%, while that of GCL-E ranges from 0.82% to 2.64%.

#### 4.5 Model Validation and Analysis

We conduct a series of ablation studies to further analyze the proposed method.

##### 4.5.1 GCL-E vs. GCL-A

Combining Tables 1 and 2, it can be observed that GCL-A does not always have inferior performance compared to GCL-E, and vice versa. The reason is that iNaturalist 2018 and Places-LT have much large imbalance ratios ( $r = 500$  and 996, respectively) than the other datasets (ImageNet-LT has the largest  $r$  which is 256 among these datasets). We draw the logit curve of different forms of GCL, which is

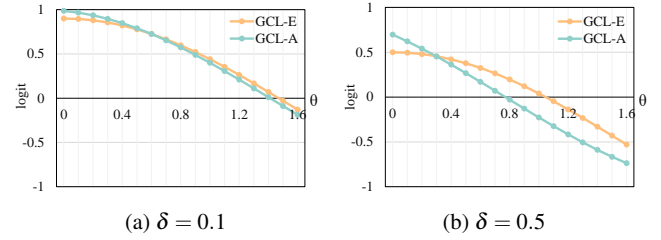


Fig. 4: The logit curve of GCL in different forms. For ease of visualization, the scale parameter  $s$  is omitted<sup>3</sup>.

shown in Fig. 4. In our setting, the large class has a small  $\delta$ . The smaller the class size, the larger its corresponding  $\delta$ . As the distance  $\theta$  increases, the logit of GCL-A decreases faster than GCL-E. It is more noticeable for the larger  $\delta$ , as shown in Fig. 4b. A small distance will have a more obvious logit difference for GCL-A compared with GCL-E. Therefore, in the case of high imbalance ratio, GCL-E can make the separability of minority classes stronger so that the logit difference is more significant. Another reason may be that cloud size selection is not only related to the class size, and each form of GCL may have its optimal cloud size selection strategy. We use the logarithmic form cloud size for GCL-A should not be the optimal one. We leave this as our future study.

##### 4.5.2 The Effect of Gaussian Cloud

To obtain additional insight, we visualize the embedding distribution using t-SNE projection. Since CE loss is selected as the loss function for several methods (Zhou et al., 2020; Kang et al., 2020; Liu et al., 2019), especially MisLAS performs the second-best in most cases, we visualize the embedding distribution obtained by CE loss for comparison. LDAM (Cao et al., 2019) is an angular distance metric based method but utilizes the hard margin, we also show its embedding distribution. The embeddings are calculated from the samples in CIFAR-10-LT with  $r = 100$ . Fig. 5 shows the results. From Fig. 5a, it can be seen that the embeddings of each class obtained via CE loss are clustered together and are relatively difficult to separate. The obscure region of CE loss embedding is larger than that of other approaches. LDAM and GCL in both forms are all angular distance metric based methods, thus their embeddings are basically radial. Fig. 5b shows that the LDAM embedding of each class is more slender. This is caused by the hard margin that strictly restricts the class region, resulting in overfitting the training set. Thus, LDAM does not generalize well on the test set compared with our proposed GCL. In Fig. 5c

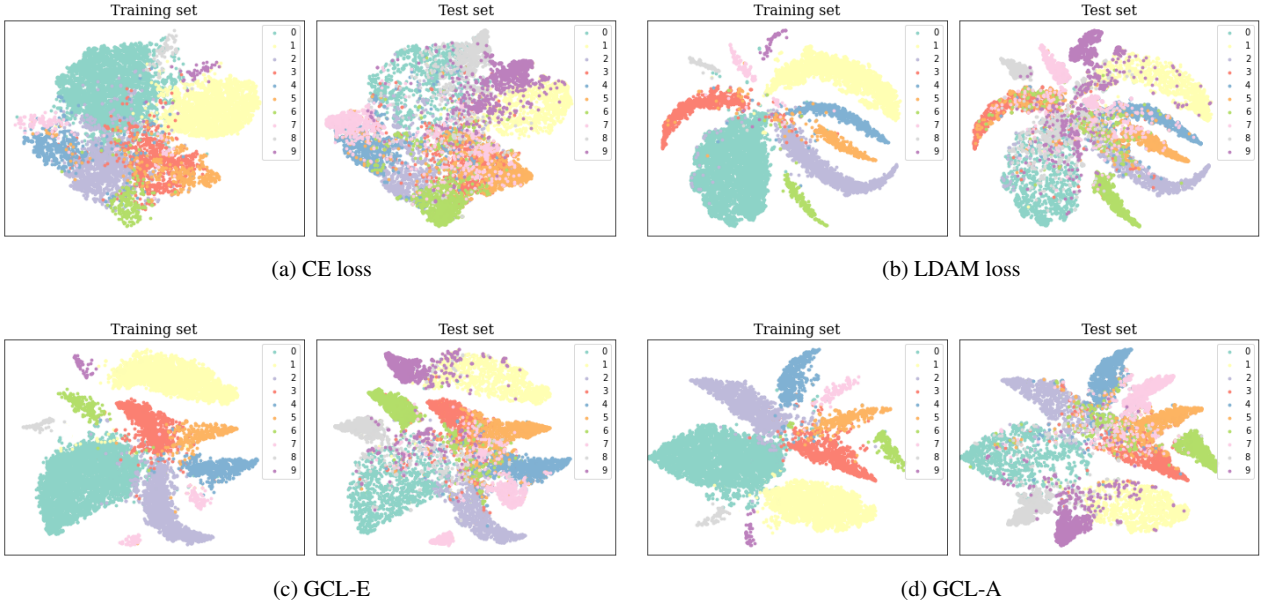
<sup>3</sup> Specifically, the logit curves show  $\bar{z}^{GCL-E} = \cos(\theta) - \delta \cdot \|\varepsilon\|$ , and  $\bar{z}^{GCL-A} = \cos(\theta + \delta \cdot \frac{\pi}{2} \cdot \|\varepsilon\|)$ , namely  $s = 1$ .

Table 3: Validation of the effect on MoE model on CIFAR-10/100-LT.

Dataset	CIFAR-10-LT			CIFAR-100-LT		
Backbone	ResNet-32					
Imbalance ratio	200	100	50	200	100	50
RIDE (Wang et al., 2021c)	80.42	83.39	85.34	47.80	50.91	54.87
RIDE w. GCL-E	81.32 ( $\uparrow 0.90$ )	84.32 ( $\uparrow 0.93$ )	87.03 ( $\uparrow 1.69$ )	48.96 ( $\uparrow 1.16$ )	52.57 ( $\uparrow 1.66$ )	57.49 ( $\uparrow 2.62$ )
RIDE w. GCL-A	82.08 ( $\uparrow 1.66$ )	84.73 ( $\uparrow 1.34$ )	86.95 ( $\uparrow 1.61$ )	48.62 ( $\uparrow 0.82$ )	52.38 ( $\uparrow 1.47$ )	57.51 ( $\uparrow 2.64$ )

Table 4: Validation of the effect on MoE model on large-scale dataset.

Dataset	ImageNet-LT	iNaturalist 2018	Places-LT
Backbone	ResNet-50	ResNet-50	ResNet-152
RIDE (Wang et al., 2021c)	55.55	72.17	39.91
RIDE w. GCL-E	57.01 ( $\uparrow 1.46$ )	74.27 ( $\uparrow 2.10$ )	41.06 ( $\uparrow 1.15$ )
RIDE w. GCL-A	57.25 ( $\uparrow 1.70$ )	73.56 ( $\uparrow 1.39$ )	41.50 ( $\uparrow 1.59$ )

Fig. 5: Visualization of the embedding distribution obtained by different methods. t-SNE projection is utilized. The dataset is CIFAR-10-LT with  $r = 100$ . ResNet-32 is used as the backbone. (Color for the best view.)

and Fig. 5d, on training set, the embeddings for each class obtained via GCL in both forms have more obvious margins compared to CE and also are more scattered compared to LDAM. The results of the test set verify the efficacy of our proposed approach. GCL-E and GCL-A have better generalization performance, and it can be found that the misclassified classes are mainly in the edge regions of each class. For better illustration, we also compare the embedding distribution of the most (class 0) and least (class 9) frequent classes obtained by different loss functions in Fig. 6. It presents more clearly that compared to our proposed GCL, the LDAM embeddings appear to perform better on the

training set, but cannot be well generalized to the unseen test samples. In Fig. 6b, there are more points of class 9 appearing inside the class 0 area on the test set. By contrast, as shown in Fig. 6c and Fig. 6d, the misclassified points of class 9 are mainly in the edge area of class 0 on test set.

#### 4.5.3 Expression of Cloud Size

We explore several different cloud size adjustment strategies, including power form with different exponents (1/3 and 1/4), and logarithmic form. For a fair comparison, we use GCL-E, and the sampler and re-training strategy are

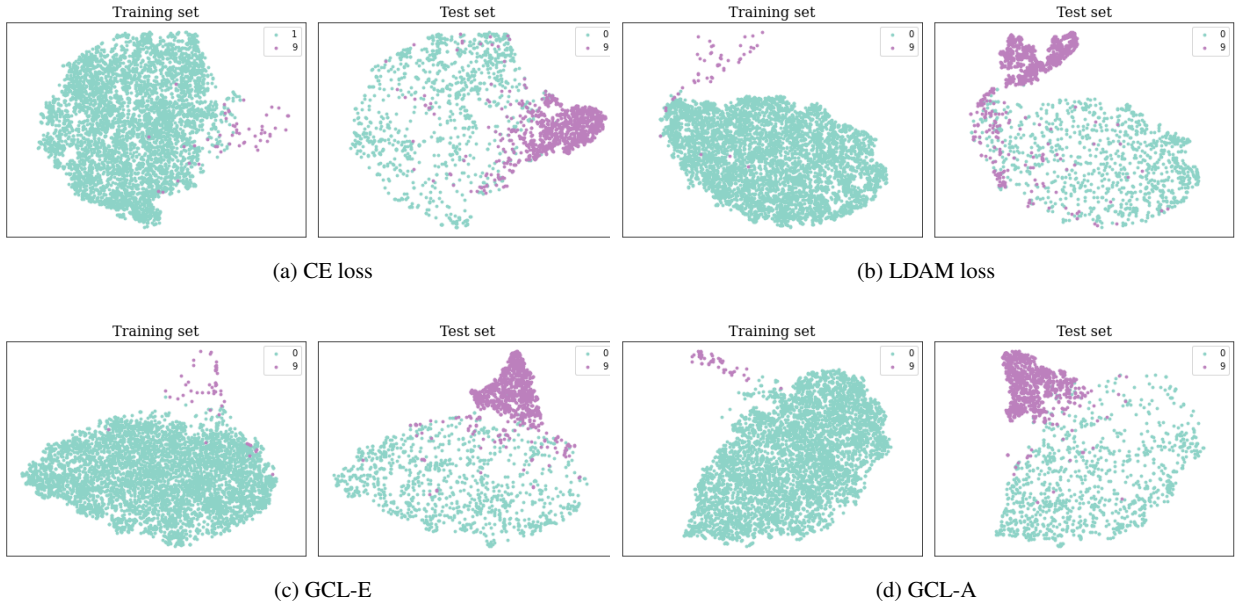


Fig. 6: T-SNE visualization of head (class 0) and tail (class 9) embedding distribution obtained by different methods. The dataset is CIFAR-10-LT with  $r = 100$ . The backbone network is ResNet-32. (Color for the best view.)

Table 5: Ablation experiment of different expression forms of cloud size ( $\delta_j^*$ ) on CIFAR-10-LT with  $r = 100$ .

$\delta_j^*$	Exp.	Expression	Acc(%)
cos.	-	$\cos(n_j/n_{max} \cdot \pi/2)$	79.21
power	1/3	$n_{max} \cdot n_j^{1/3}$	80.80
power	1/4	$n_{max} \cdot n_j^{-1/4}$	82.31
log.	-	$\log n_{max} - \log n_j$	<b>82.73</b>

selected as class-balanced sampling and cRT, respectively. The results are presented in Table 5. The logarithmic form has the best performance and the power form with the exponent of 1/4 is also competitive.

#### 4.5.4 Strategies for balanced Sampling

We implement different strategies of data re-sampling to better analyze our proposed method. The re-sampling strategy (sampler) includes instance-balanced sampler (IBS) (Kang et al., 2020), square-root sampler (SRS) (Mahajan et al., 2018), effective number sampler (ENS) (Cui et al., 2019) and class balanced-sampler (CBS) (Kang et al., 2020). The form of GCL is GCL-E and the re-training techniques for all samplers are cRT. Table 6 shows the results. IBS decreases the performance slightly (from 80.55% to 80.52%), which indicates that training the classifier with IBS leads to classifier overfitting. CRT improves the model performance because it increases the sampling probability of tail classes. ENS and CBS have better performance because they can

address the problem of negative gradient over suppression by balancing the amount of data in each class. We use CBS in the comparison experiments because it achieves the best results among these samplers.

#### 4.5.5 Technique for Balancing Classifier

For the selection of classifier re-training (RT) technique, we first train the backbone without any RT technology using GCL-E. Then we froze the representation and re-balance the classifier with learnable weight scaling (LWS),  $\tau$ -normalized classifier ( $\tau$ -NC), and cRT, respectively. Table 7 presents the top-1 accuracy on CIFAR-10-LT with  $r = 100$ . We can observe that even without any RT technique, our approach (the top-1 classification accuracy is 80.55%) can still beat most state-of-the-art including two-stage methods (for example, LDAM-DRW and BBN achieve 77.03% and 79.82%, respectively). All RT techniques significantly improve model performance, which demonstrates that good representation can improve classification accuracy by simply re-balancing the classifier. cRT outperforms best among the classifier re-training techniques, which improves the accuracy by 2.18% compared with no RT. Thus, we use cRT in the comparison experiments.

#### 4.5.6 Performance on Classes with Different Scale

To investigate the impact of GCL, we report the accuracy of various scale classes on ImageNet-LT. The results are presented in Table 8. The classification accuracy of baseline

Table 6: Ablation experiment of different re-sampling strategy on CIFAR-10-LT with  $r = 100$ .

Sampler	RT tech.	Acc. (%)
IBS	cRT	80.52
SRT	cRT	81.74
ENS	cRT	82.45
CBS	cRT	<b>82.73</b>

Table 7: Ablation experiment of different re-training techniques on CIFAR-10-LT with  $r = 100$ .

Sampler	RT tech.	Acc. (%)
-	without RT	80.55
CBS	LWS	82.25
CBS	$\tau$ -NC	82.16
CBS	cRT	<b>82.73</b>

Table 8: Top-1 Classification Accuracy (%) of the three splits on ImageNet-LT.

Method	Head	Middle	Tail	All
Class size	$n_j > 100$	$20 < n_j \leq 100$	$n_j \leq 20$	-
CE	<b>64.91</b>	38.10	11.28	44.51
CosFace	64.48	39.26	11.55	44.95
ArcFace	<b>64.86</b>	38.07	11.75	44.54
LDAM-DRW	58.63	48.95	30.37	49.96
OLTR	61.93	44.68	19.98	47.72
Decoupling	63.71	43.01	20.55	47.70
MisLAS	62.43	49.31	33.89	52.11
GCL-E	63.78	<b>52.62</b>	<b>38.70</b>	<b>54.84</b>
GCL-A	62.72	<b>53.26</b>	<b>40.95</b>	<b>55.12</b>

methods drops a lot in the middle and tail classes. LDAM-DRW increases the accuracy of middle and tail classes but decreases that of head classes a lot. GCL-E outperforms the other state-of-the-art methods on middle and tail classes with large margins. Meanwhile, the accuracy of the head class decreases the least. By contrast, GCL-A has more improvement in middle and tail classes, but the damage to head classes is slightly higher than GCL-E and decoupling. In general, GCL-E performs well in all class scales. GCL-A has the highest overall classification accuracy. Significantly improving the accuracy of tail classes while preventing that of the head classes from diminishing illustrates the superiority of our approach.

## 5 Conclusion

In this paper, we have proposed to use Gaussian form perturbation to augment the features for long-tailed classification. Eventually, we have derived two GCL forms, which are simple but effective. Both of these two forms

make tail classes have larger perturbation amplitudes on their corresponding class anchors, which can expand the spatial distribution of tail class embeddings. Furthermore, we have analyzed the rationale of the proposed method from different perspectives, which provides insights into how to obtain a representative and balanced-distributed embedding. After obtaining a balanced distributed embedding space, the classifier bias can be effectively addressed by simply retraining it with class-balanced sampling. Comprehensive experiments on various benchmark datasets have demonstrated that the proposed Gaussian clouded logit in both forms achieves significant performance gains compared to the state-of-the-art methods. In addition, we have also validated the properties of the proposed GCL by t-SNE visualization and the performance on different scales of classes.

**Data Availability** Public code availability: <https://github.com/Keke921/GCLLoss>

## References

Kaiming He, Xiangyu Zhang, Shaoqing Ren, and Jian Sun. Deep residual learning for image recognition. In *Proceedings of the IEEE/CVF Conference on Computer Vision and Pattern Recognition*, pages 770–778, 2016.

Feng Wang, Xiang Xiang, Jian Cheng, and Alan Loddon Yuille. Normface:  $L_2$  hypersphere embedding for face verification. In *Proceedings of the ACM International Conference on Multimedia*, pages 1041–1049, 2017a.

Pang Jiangmiao, Kai Chen, Qi Li, Zihai Xu, Huajun Feng, Jianping Shi, Wanli Ouyang, and Dahua Lin. Towards balanced learning for instance recognition. *International Journal of Computer Vision*, 129(5):1376–1393, 2021.

Maurice G Kendall et al. *The advanced theory of statistics*. Charles Griffin and Co., Ltd., 42 Drury Lane, London, 1948.

Aaron Clauset, Cosma Rohilla Shalizi, and Mark EJ Newman. Power-law distributions in empirical data. *SIAM Review*, 51(4):661–703, 2009.

Lu Yang, He Jiang, Qing Song, and Jun Guo. A survey on long-tailed visual recognition. *International Journal of Computer Vision*, 130(7):1837–1872, 2022.

Yuhang Zang, Kaiyang Zhou, Chen Huang, and Chen Change Loy. Semi-supervised and long-tailed object detection with cascadematch. *International Journal of Computer Vision*, 131(4):987–1001, 2023.

Kunzhe Huang, Yiming Li, Baoyuan Wu, Zhan Qin, and Kui Ren. Backdoor defense via decoupling the training process. In *Proceedings of the International Conference on Learning Representations*, pages 1–25, 2022.

Mengnan Du, Subhabrata Mukherjee, Guanchu Wang, Ruixiang Tang, Ahmed Awadallah, and Xia Hu. Fairness

via representation neutralization. *Advances in Neural Information Processing Systems*, 34:12091–12103, 2021.

De-Wang Li and Hua Huang. Few-shot class-incremental learning via compact and separable features for fine-grained vehicle recognition. *IEEE Transactions on Intelligent Transportation Systems*, pages 1–12, 2022.

Defang Chen, Jian-Ping Mei, Hailin Zhang, Can Wang, Yan Feng, and Chun Chen. Knowledge distillation with the reused teacher classifier. In *Proceedings of the IEEE/CVF Conference on Computer Vision and Pattern Recognition*, pages 11933–11942, 2022.

Boyan Zhou, Quan Cui, Xiu-Shen Wei, and Zhao-Min Chen. BBN: Bilateral-branch network with cumulative learning for long-tailed visual recognition. In *Proceedings of the IEEE/CVF Conference on Computer Vision and Pattern Recognition*, pages 9719–9728, 2020.

Bingyi Kang, Saining Xie, Marcus Rohrbach, Zhicheng Yan, Albert Gordo, Jiashi Feng, and Yannis Kalantidis. Decoupling representation and classifier for long-tailed recognition. In *Proceedings of the International Conference on Learning Representations*, pages 1–16, 2020.

Kaidi Cao, Colin Wei, Adrien Gaidon, Nikos Arechiga, and Tengyu Ma. Learning imbalanced datasets with label-distribution-aware margin loss. In *Advances in Neural Information Processing Systems*, pages 1567–1578, 2019.

Tao Wang, Yu Li, Bingyi Kang, Junnan Li, Junhao Liew, Sheng Tang, Steven Hoi, and Jiashi Feng. The devil is in classification: A simple framework for long-tail instance segmentation. In *Proceedings of the European Conference on Computer Vision*, pages 728–744, 2020a.

Songyang Zhang, Zeming Li, Shipeng Yan, Xuming He, and Jian Sun. Distribution alignment: A unified framework for long-tail visual recognition. In *Proceedings of the IEEE/CVF Conference on Computer Vision and Pattern Recognition*, pages 2361–2370, 2021a.

Laurens Van der Maaten and Geoffrey Hinton. Visualizing data using t-SNE. *Journal of Machine Learning Research*, 9(11):2579–2605, 2008.

Linda B Smith and Lauren K Slone. A developmental approach to machine learning? *Frontiers in Psychology*, 8:2124, 2017.

Yin Cui, Menglin Jia, Tsung-Yi Lin, Yang Song, and Serge Belongie. Class-balanced loss based on effective number of samples. In *Proceedings of the IEEE/CVF Conference on Computer Vision and Pattern Recognition*, pages 9268–9277, 2019.

Chen Huang, Yining Li, Chen Change Loy, and Xiaoou Tang. Learning deep representation for imbalanced classification. In *Proceedings of the IEEE/CVF Conference on Computer Vision and Pattern Recognition*, pages 5375–5384, 2016.

Yu-Xiong Wang, Deva Ramanan, and Martial Hebert. Learning to model the tail. *Advances in Neural Information Processing Systems*, 30:7029–7039, 2017b.

Dhruv Mahajan, Ross Girshick, Vignesh Ramanathan, Kaiming He, Manohar Paluri, Yixuan Li, Ashwin Bharambe, and Laurens van der Maaten. Exploring the limits of weakly supervised pretraining. In *Proceedings of the European Conference on Computer Vision*, volume 11206, pages 185–201, 2018.

Yin Cui, Yang Song, Chen Sun, Andrew Howard, and Serge J. Belongie. Large scale fine-grained categorization and domain-specific transfer learning. In *Proceedings of the IEEE/CVF Conference on Computer Vision and Pattern Recognition*, pages 4109–4118, 2018.

Mengke Li, Yiu-ming Cheung, and Yang Lu. Long-tailed visual recognition via gaussian clouded logit adjustment. In *Proceedings of the IEEE/CVF Conference on Computer Vision and Pattern Recognition*, pages 6929–6938, 2022a.

Christian Szegedy, Wei Liu, Yangqing Jia, Pierre Sermanet, Scott E. Reed, Dragomir Anguelov, Dumitru Erhan, Vincent Vanhoucke, and Andrew Rabinovich. Going deeper with convolutions. In *Proceedings of the IEEE/CVF Conference on Computer Vision and Pattern Recognition*, pages 1–9, 2015.

Jianfeng Wang, Thomas Lukasiewicz, Xiaolin Hu, Jianfei Cai, and Xu Zhenghua. RSG: A simple but effective module for learning imbalanced datasets. In *Proceedings of the IEEE/CVF Conference on Computer Vision and Pattern Recognition*, pages 3784–3793, 2021a.

Jaehyung Kim, Jongheon Jeong, and Jinwoo Shin. M2m: Imbalanced classification via major-to-minor translation. In *Proceedings of the IEEE/CVF Conference on Computer Vision and Pattern Recognition*, pages 13896–13905, 2020.

Xi Yin, Xiang Yu, Kihyuk Sohn, Xiaoming Liu, and Manmohan Chandraker. Feature transfer learning for face recognition with under-represented data. In *Proceedings of the IEEE/CVF Conference on Computer Vision and Pattern Recognition*, pages 5704–5713, 2019.

Jialun Liu, Yifan Sun, Chuchu Han, Zhaopeng Dou, and Wenhui Li. Deep representation learning on long-tailed data: A learnable embedding augmentation perspective. In *Proceedings of the IEEE/CVF Conference on Computer Vision and Pattern Recognition*, pages 2967–2976, 2020.

Bolei Zhou, Aditya Khosla, Àgata Lapedriza, Aude Oliva, and Antonio Torralba. Learning deep features for discriminative localization. In *Proceedings of the IEEE/CVF Conference on Computer Vision and Pattern Recognition*, pages 2921–2929, 2016.

Peng Chu, Xiao Bian, Shaopeng Liu, and Haibin Ling. Feature space augmentation for long-tailed data. In

*Proceedings of the European Conference on Computer Vision*, volume 12374, pages 694–710, 2020.

Yongshun Zhang, Xiu-Shen Wei, Boyan Zhou, and Jianxin Wu. Bag of tricks for long-tailed visual recognition with deep convolutional neural networks. In *Proceedings of the AAAI Conference on Artificial Intelligence*, pages 3447–3455, 2021b.

Xin Wang, Thomas E. Huang, Joseph Gonzalez, Darrell Trevor, and Fisher Yu. Frustratingly simple few-shot object detection. In *Proceedings of the International Conference on Machine Learning*, volume 119, pages 9919–9928, 2020b.

Zhisheng Zhong, Jiequan Cui, Shu Liu, and Jiaya Jia. Improving calibration for long-tailed recognition. In *Proceedings of the IEEE/CVF Conference on Computer Vision and Pattern Recognition*, pages 16489–16498, 2021.

Vikas Verma, Alex Lamb, Christopher Beckham, Amir Najafi, Ioannis Mitliagkas, David Lopez-Paz, and Yoshua Bengio. Manifold mixup: Better representations by interpolating hidden states. In *Proceedings of the International Conference on Machine Learning*, pages 6438–6447, 2019.

Peng Wang, Kai Han, Xiu-Shen Wei, Lei Zhang, and Lei Wang. Contrastive learning based hybrid networks for long-tailed image classification. In *Proceedings of the IEEE/CVF Conference on Computer Vision and Pattern Recognition*, pages 943–952, 2021b.

Yu Li, Tao Wang, Bingyi Kang, Sheng Tang, Chunfeng Wang, Jintao Li, and Jiashi Feng. Overcoming classifier imbalance for long-tail object detection with balanced group softmax. In *Proceedings of the IEEE/CVF Conference on Computer Vision and Pattern Recognition*, pages 10991–11000, 2020.

Liuyu Xiang, Guiguang Ding, and Jungong Han. Learning from multiple experts: Self-paced knowledge distillation for long-tailed classification. In *Proceedings of the European Conference on Computer Vision*, pages 247–263, 2020.

Jiarui Cai, Yizhou Wang, and Jenq-Neng Hwang. Ace: Ally complementary experts for solving long-tailed recognition in one-shot. In *Proceedings of the International Conference on Computer Vision*, pages 112–121, 2021.

Jiequan Cui, Shu Liu, Zhuotao Tian, Zhisheng Zhong, and Jiaya Jia. Reslt: Residual learning for long-tailed recognition. *IEEE Transactions on Pattern Analysis and Machine Intelligence*, 45(3):3695–3706, 2023.

Xudong Wang, Long Lian, Zhongqi Miao, Ziwei Liu, and Stella X. Yu. Long-tailed recognition by routing diverse distribution-aware experts. In *Proceedings of the International Conference on Learning Representations*, pages 1–16, 2021c.

Bolian Li, Zongbo Han, Haining Li, Huazhu Fu, and Changqing Zhang. Trustworthy long-tailed classification. In *Proceedings of the IEEE/CVF Conference on Computer Vision and Pattern Recognition*, pages 6970–6979, 2022b.

Yan Jin, Mengke Li, Yang Lu, Yiu-ming Cheung, and Hanzi Wang. Long-tailed visual recognition via self-heterogeneous integration with knowledge excavation. In *Proceedings of the IEEE/CVF Conference on Computer Vision and Pattern Recognition*, early access, 2023.

Jun Li, Zichang Tan, Jun Wan, Zhen Lei, and Guodong Guo. Nested collaborative learning for long-tailed visual recognition. In *Proceedings of the IEEE/CVF Conference on Computer Vision and Pattern Recognition*, pages 6949–6958, 2022c.

Jiequan Cui, Zhisheng Zhong, Shu Liu, Bei Yu, and Jiaya Jia. Parametric contrastive learning. In *Proceedings of the International Conference on Computer Vision*, pages 715–724, 2021.

Mengye Ren, Wenyuan Zeng, Bin Yang, and Raquel Urtasun. Learning to reweight examples for robust deep learning. In *Proceedings of the International Conference on Machine Learning*, volume 80, pages 4331–4340, 2018.

Tsung-Yi Lin, Priya Goyal, Ross B. Girshick, Kaiming He, and Piotr Dollár. Focal loss for dense object detection. *IEEE Transactions on Pattern Analysis and Machine Intelligence*, 42(2):318–327, 2020.

Salman H. Khan, Munawar Hayat, Mohammed Bennamoun, Ferdous Ahmed Sohel, and Roberto Togneri. Cost-sensitive learning of deep feature representations from imbalanced data. *IEEE Transactions on Neural Networks and Learning Systems*, 29(8):3573–3587, 2018.

Jingru Tan, Changbao Wang, Buyu Li, Quanquan Li, Wanli Ouyang, Changqing Yin, and Junjie Yan. Equalization loss for long-tailed object recognition. In *Proceedings of the IEEE/CVF Conference on Computer Vision and Pattern Recognition*, pages 11659–11668, 2020.

Saptarshi Sinha, Hiroki Ohashi, and Katsuyuki Nakamura. Class-difficulty based methods for long-tailed visual recognition. *International Journal of Computer Vision*, 130(10):2517–2531, 2022.

Pang Wei Koh and Percy Liang. Understanding black-box predictions via influence functions. In *Proceedings of the International Conference on Machine Learning*, volume 70 of *Proceedings of Machine Learning Research*, pages 1885–1894, 2017.

Aditya Krishna Menon, Sadeep Jayasumana, Ankit Singh Rawat, Himanshu Jain, Andreas Veit, and Sanjiv Kumar. Long-tail learning via logit adjustment. In *Proceedings of the International Conference on Learning Representations*, pages 1–27, 2021.

Youngkyu Hong, Seungju Han, Kwanghee Choi, Seokjun Seo, Beomsu Kim, and Buru Chang. Disentangling label distribution for long-tailed visual recognition. In *Proceedings of the IEEE/CVF Conference on Computer Vision and Pattern Recognition*, pages 6626–6636, 2021.

Dong Cao, Xiangyu Zhu, Xingyu Huang, Jianzhu Guo, and Zhen Lei. Domain balancing: Face recognition on long-tailed domains. In *Proceedings of the IEEE/CVF Conference on Computer Vision and Pattern Recognition*, pages 5670–5678, 2020.

Mengke Li, Yiu-ming Cheung, and Zhikai Hu. Key point sensitive loss for long-tailed visual recognition. *IEEE Transactions on Pattern Analysis and Machine Intelligence*, 45(4):4812–4825, 2023.

Hao Wang, Yitong Wang, Zheng Zhou, Xing Ji, Dihong Gong, Jingchao Zhou, Zhifeng Li, and Wei Liu. Cosface: Large margin cosine loss for deep face recognition. In *Proceedings of the IEEE/CVF Conference on Computer Vision and Pattern Recognition*, pages 5265–5274, 2018.

Jiankang Deng, Jia Guo, Niannan Xue, and Stefanos Zafeiriou. Arcface: Additive angular margin loss for deep face recognition. In *Proceedings of the IEEE/CVF Conference on Computer Vision and Pattern Recognition*, pages 4690–4699, 2019.

Pascal Vincent, Hugo Larochelle, Yoshua Bengio, and Pierre-Antoine Manzagol. Extracting and composing robust features with denoising autoencoders. In *Proceedings of the International Conference on Machine Learning*, pages 1096–1103, 2008.

Tiago S. Nazaré, Gabriel B. Paranhos da Costa, Welinton A. Contato, and Moacir Ponti. Deep convolutional neural networks and noisy images. In *Progress in Pattern Recognition, Image Analysis, Computer Vision, and Applications*, volume 10657, pages 416–424, 2018.

Jaehun Kim, Stjepan Picek, Annelie Heuser, Shivam Bhasin, and Alan Hanjalic. Make some noise. unleashing the power of convolutional neural networks for profiled side-channel analysis. *IACR Transactions on Cryptographic Hardware and Embedded Systems*, 2019(3):148–179, 2019.

Wilfrid J. MDixon and Frank J. Massey Jr. *Introduction to statistical analysis*. McGraw-Hill, 1951.

R Lyman Ott and Micheal T Longnecker. *An introduction to statistical methods and data analysis*. Cengage Learning, Brooks/Cole, 20 Channel Center Street, Boston, MA 02210, USA, 7 edition, 2015.

Carl Rasmussen. The infinite gaussian mixture model. *Advances in Neural Information Processing Systems*, 12: 554–560, 1999.

William Mendenhall, Robert J. Beaver, and Barbara M. Beaver. *Introduction to probability and statistics*. Cengage Learning, Richard Stratton, Brooks/Cole, 20 Channel Center Street, Boston, MA 02210, USA, 14 edition, 2013.

Binghui Chen, Weihong Deng, and Junping Du. Noisy softmax: Improving the generalization ability of dcnn via postponing the early softmax saturation. In *Proceedings of the IEEE/CVF Conference on Computer Vision and Pattern Recognition*, pages 4021–4030, 2017.

Wanping Zhang, Yongru Chen, Wenming Yang, Guijin Wang, Jing-Hao Xue, and Qingmin Liao. Class-variant margin normalized softmax loss for deep face recognition. *IEEE Transactions on Neural Networks and Learning Systems*, 32(10):4742–4747, 2021c.

Colin Wei and Tengyu Ma. Improved sample complexities for deep neural networks and robust classification via an all-layer margin. In *Proceedings of the International Conference on Learning Representations*, pages 1–37, 2020.

Jiaqi Wang, Wenwei Zhang, Yuhang Zang, Yuhang Cao, Jiangmiao Pang, Tao Gong, Kai Chen, Ziwei Liu, Chen Change Loy, and Dahua Lin. Seesaw loss for long-tailed instance segmentation. In *Proceedings of the IEEE/CVF Conference on Computer Vision and Pattern Recognition*, pages 9695–9704, Virtual Event, 2021d.

Tong Wang, Yousong Zhu, Chaoyang Zhao, Wei Zeng, Jin-qiao Wang, and Ming Tang. Adaptive class suppression loss for long-tail object detection. In *Proceedings of the IEEE/CVF Conference on Computer Vision and Pattern Recognition*, pages 3103–3112, Virtual Event, 2021e.

Alex Krizhevsky, Geoffrey Hinton, et al. Learning multiple layers of features from tiny images. *Tech Report*, 2009.

Olga Russakovsky, Jia Deng, Hao Su, Jonathan Krause, Sanjeev Satheesh, Sean Ma, Zhiheng Huang, Andrej Karpathy, Aditya Khosla, Michael Bernstein, Alexander C. Berg, and Fei-Fei Li. Imagenet large scale visual recognition challenge. *International Journal of Computer Vision*, 115(3):211–252, 2015.

Bolei Zhou, Agata Lapedriza, Aditya Khosla, Aude Oliva, and Antonio Torralba. Places: A 10 million image database for scene recognition. *IEEE Transactions on Pattern Analysis and Machine Intelligence*, 40(6):1452–1464, 2017.

Ziwei Liu, Zhongqi Miao, Xiaohang Zhan, Jiayun Wang, Boqing Gong, and Stella X. Yu. Large-scale long-tailed recognition in an open world. In *Proceedings of the IEEE/CVF Conference on Computer Vision and Pattern Recognition*, pages 2537–2546, 2019.

Grant Van Horn, Oisin Mac Aodha, Yang Song, Yin Cui, Chen Sun, Alex Shepard, Hartwig Adam, Pietro Perona, and Serge J. Belongie. The inaturalist species classification and detection dataset. In *Proceedings of the IEEE/CVF Conference on Computer Vision and Pattern Recognition*, pages 8769–8778, 2018.

Rajeev Ranjan, Carlos Domingo Castillo, and Rama Chellappa. L2-constrained softmax loss for discriminative

face verification. *ArXiv*, abs/1703.09507:1–10, 2017.

Hongyi Zhang, Moustapha Cisse, Yann N Dauphin, and David Lopez-Paz. mixup: Beyond empirical risk minimization. *Proceedings of the International Conference on Learning Representations*, pages 1–13, 2018.

Adam Paszke, Sam Gross, Francisco Massa, Adam Lerer, James Bradbury, Gregory Chanan, Trevor Killeen, Zeming Lin, Natalia Gimelshein, Luca Antiga, et al. Pytorch: An imperative style, high-performance deep learning library. *Advances in Neural Information Processing Systems*, 32:8024–8035, 2019.

Kaihua Tang, Jianqiang Huang, and Hanwang Zhang. Long-tailed classification by keeping the good and removing the bad momentum causal effect. *Advances in Neural Information Processing Systems*, 33:1513–1524, 2020.

Tianhong Li, Peng Cao, Yuan Yuan, Lijie Fan, Yuzhe Yang, Rogerio S. Feris, Piotr Indyk, and Dina Katabi. Targeted supervised contrastive learning for long-tailed recognition. In *Proceedings of the IEEE/CVF Conference on Computer Vision and Pattern Recognition*, pages 6918–6928, 2022d.

Jialun Liu, Wenhui Li, and Yifan Sun. Memory-based jitter: Improving visual recognition on long-tailed data with diversity in memory. In *Proceedings of the AAAI Conference on Artificial Intelligence*, pages 1720–1728, 2022.

Mengke Li, Yiu-ming Cheung, and Juyong Jiang. Feature-balanced loss for long-tailed visual recognition. In *IEEE International Conference on Multimedia and Expo*, pages 1–6, 2022e.

Yu-Jhe Li, Fu-En Yang, Yen-Cheng Liu, Yu-Ying Yeh, Xiaofei Du, and Yu-Chiang Frank Wang. Adaptation and re-identification network: An unsupervised deep transfer learning approach to person re-identification. In *Proceedings of the IEEE/CVF Conference on Computer Vision and Pattern Recognition Workshop*, pages 172–178, 2018.

Ruibing Hou, Bingpeng Ma, Hong Chang, Xinqian Gu, Shiguang Shan, and Xilin Chen. VRSTC: Occlusion-free video person re-identification. In *Proceedings of the IEEE/CVF Conference on Computer Vision and Pattern Recognition*, pages 7183–7192, 2019.

Mei Wang and Weihong Deng. Deep face recognition: A survey. *Neurocomputing*, 429:215–244, 2021.